# Reflective silicon binary diffraction grating for visible wavelengths

**Zhen Peng,[1] David A. Fattal,[1,2] Andrei Faraon,[1] Marco Fiorentino,[1,3] Jingjing Li,[1] and Raymond G. Beausoleil[1]**

[1]*Hewlett-Packard Laboratories, 1501 Page Mill Road, Palo Alto, California 94304, USA*

[2]*e-mail: david.fattal@hp.com*

[3]*e-mail: marco.fiorentino@hp.com*

Received January 31, 2011; revised March 17, 2011; accepted March 19, 2011;
posted March 21, 2011 (Doc. ID 141947); published April 15, 2011

We introduce a device based on subwavelength resonant grating technology. Using a single lithography step we built a reflective binary grating that mimics the functionality of a blazed diffraction grating in a flat geometry. We have also demonstrated that efficient subwavelength resonant devices for visible wavelengths can be built using silicon.

*OCIS codes:* 050.2770, 050.6624.

Dielectric gratings with subwavelength features made of high-index material, such as silicon, can exhibit internal resonances that profoundly affect their far-field properties [1]. A periodic pattern of high-index grooves with subwavelength thickness and period, for instance, can reflect light almost perfectly in a broad spectral range [2], whereas an effective medium approach would predict only a small amount of reflection [3]. A new type of broadband dielectric mirror has been engineered based on this effect, and has been shown to perform better than standard dielectric stacks as a top reflector in a vertical-cavity surface-emitting laser [4].

Recently our group introduced a remarkable property of high-index grating mirrors [5]: the ability to fully control the phase front of the reflected beam by using a carefully chosen, nonperiodic patterning of the grating. We used that property to fabricate a focusing mirror made of a thin silicon layer on an oxide substrate with a binary groove pattern, i.e., a pattern that can be built with a single lithographic step. A theoretical analysis of similar devices [6] confirmed the effect.

In this Letter, we use our resonance grating technology to design reflective diffraction gratings with high efficiency in a particular diffraction order. The conventional way to achieve high diffraction efficiencies is to use blazed groove patterns, which require either mechanical ruling or complex lithography for their manufacture. In addition, blazed gratings suffer from detrimental shadowing effects—neighboring grooves blocking the path of the diffracted wave—which ultimately limit their efficiency. Here instead we use a binary reflection grating that, albeit flat, mimics blazing via a linear spatial phase gradient of its reflection coefficient [7]. Our analysis also demonstrates that very efficient diffractive elements can be realized with lossy grating materials (here, silicon at 650 nm wavelength) since we show that a $2\pi$ phase differential can be achieved even for a subwavelength grating thickness.

Guided mode resonance (GMR) devices are based on subwavelength binary gratings that consist of a single layer of high-index dielectric (such as silicon) sandwiched between two lower index dielectrics (such as quartz and air). A grating is etched in this layer using a single lithography step. The grating is designed to be able to guide light inside the high-index layer. The guided modes are scattered by the grating and, for an appropriate choice of the grating parameters, one can observe resonances in the guided mode. These resonances scatter light back in the free-space modes and, therefore, provide a way to engineer the grating reflectivity and transmissivity [8].

We recognized that the phase response associated with the resonantly scattered light can be used to control the phase front of the reflected light [5] and, therefore, build flat optical devices that act as nonplanar mirrors. Our initial experiments concentrated on near-infrared wavelengths for which silicon is transparent. One would expect silicon GMR gratings not to work in the visible range because of the strong absorption of silicon at those wavelengths. Figure 1 instead shows that, if one chooses a thin (180 nm) silicon layer to build the grating, reflectivity in excess of 80% can be obtained for TM polarized

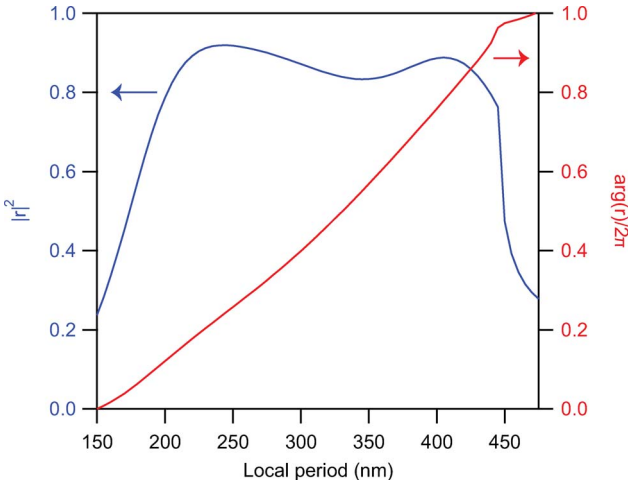


Fig. 1. (Color online) Plot of the argument (blue) and normalized phase (red) of the reflection coefficient $r$ into the zeroth order (normal to the surface) of a high contrast grating as a function of the period (TM polarization) calculated using RCWA. Below 450 nm the zeroth order is the only allowed order for the subwavelength grating; the onset of the first diffracted order at 450 nm shows up as a sudden drop of reflectivity. The silicon grooves ($n = 3.48$) are located on quartz substrate ($n = 1.46$), with a thickness of 170 nm, a duty cycle of 50%. The design wavelength is 650 nm.

 

light at 650 nm. Figure 1 also shows that, by changing the grating period, the phase of the reflected beam can span an interval of $2\pi$ with a small loss in reflectivity. Higher-reflectivity designs can be found but they require small feature size that cannot be easily fabricated.

To understand how to obtain an effective blazing effect with a GMR grating, let us consider initially the phase delay introduced by a flat mirror tilted by an angle $\theta_0/2$ about the $y$-axis:

$$\Phi_M(x,y,\lambda) = \frac{2\pi \sin\theta_0}{\lambda} x. \tag{1}$$

Note that $\lambda\nabla\Phi$ is constant for all wavelengths, so that all wavelengths are deflected identically. In the case of a GMR mirror we can design the phase profile for a given wavelength $\lambda_0$ to be

$$\Phi_0(x,y) = \frac{2\pi \sin\theta_0}{\lambda_0} x. \tag{2}$$

This would give the same amount of deviation as a tilted mirror for the wavelength $\lambda_0$. Based on Eq.(2), we can design a GMR dispersion grating of period $\Lambda$ and blaze angle $\theta_0/2$ by defining the phase profile of the mirror to be

$$\Phi_B(x,y,\lambda_0) = \frac{2\pi \sin\theta_0}{\lambda_0} (x \mathrm{mod} \Lambda). \tag{3}$$

This phase profile is schematically shown as the black curve in the top graph of Fig. 2(a). Assuming a flat reflectivity profile, the complex reflection coefficient of the grating is given simply by $r_B = \exp(i\Phi_B)$. In general, $r_B$ contains several Fourier coefficients, giving rise to scattering in several diffraction orders. However, for particular values $\theta_m/2$ of the blaze angle given by $\sin(\theta_m) = m\lambda_0/\Lambda$, only the $m$th Fourier coefficient is present, and 100% of the scattering happens in diffraction order $m$.

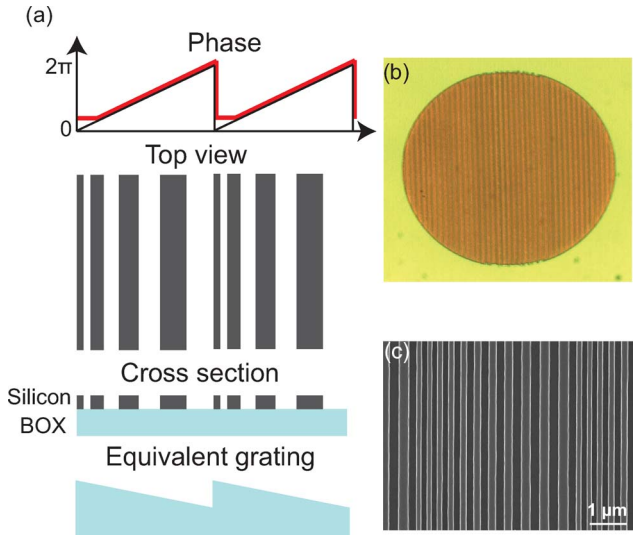


Fig. 2. (Color online) (a) Top figure shows, in black, the ideal blazed grating phase profile and, in red, the design profile we used. Below the phase profile we have schematic top view and cross section of a binary reflection grating that implements the blazed phase profile. In the bottom, the equivalent 3D grating cross section. (b) Microphotograph of a 150 $\mu$m binary reflection grating. (c) SEM picture of the grating grooves showing the modulation in the period.

Standard blazed diffraction gratings use a 3D groove shape to achieve the target phase profile [see bottom picture of Fig. 2(a)]. They are more complex to fabricate than binary gratings, and suffer from shadowing effects, which limits their efficiencies in practice. Instead, using the spatial modulation of GMRs, we can build a phase profile that mimics an optimal blazed grating for the first diffracted order. We chose to design gratings operating with TM polarization at 650 nm wavelength in a first-order diffraction angle $\theta_1 = 10°$. For crystalline silicon, we found that the optimum grating thickness was in the range 160–180 nm, thin enough to greatly reduce the effects of silicon absorption. To obtain a full $2\pi$ phase range we would need to build grooves that are less than 100 nm wide. This fabrication task cannot be accomplished using the lithography and etching tools at our disposal, so we designed a grating that has the phase profile shown by the red curve in the top graph of Fig. 2(a). The "flat" region at the bottom of the phase profile allows us to avoid narrow grooves, but as we show below it contributes to diffraction in the zeroth order of the grating (specular reflection). A simulation of the scattering efficiency of the grating with a flattened phase profile showing this effect is reported in Table 1. The phase gradient can in principle be implemented using a combination of duty cycle and local period variation as explained in [5]. Here we varied the local period only since we found it gave the largest feature sizes and was easiest for fabrication. The complex reflection coefficient of a 170 nm thick grating was computed using the rigorous coupled-wave analysis (RCWA) method [9], and is shown in Fig. 1 as a function of local period. A phase differential of $1.5\pi$ can be obtained within the high-reflection window, and a remaining $0.5\pi$ fall in a lower reflectivity region. In principle, a better design can be found with smaller feature sizes; our choice was a good compromise for a conceptual demonstration given our fabrication abilities.

Device fabrication starts with a silicon on oxide wafer with 250 nm silicon and 3 $\mu$m buried oxide. First, the top silicon layer is thinned down to 180 nm by thermal oxidation. After removing the oxide in buffered oxide etchant, we apply polymethyl methacrylate (PMMA) resist on the wafer and use electron-beam lithography to pattern the grating structures. The developed PMMA pattern undergoes a weak oxygen descum to remove resist residues. Finally, the silicon grating is etched in HBr plasma using an Oxford reactive ion etcher. Figure 2(b) shows a

**Table 1. Theoretical and Experimental Power Distribution among Diffraction Orders of the Binary Reflection Grating[a]**

| | Order | | | | |
|---|---|---|---|---|---|
| | −2 | −1 | 0 | 1 | 2 |
| Theory | 0.068 | 0.11 | 0.155 | 0.44 | 0.009 |
| Experiment | 0.014 | 0.014 | 0.14 | 0.39 | 0.019 |

[a]The theory is for 650 nm while the experiment was carried out at 640 nm.

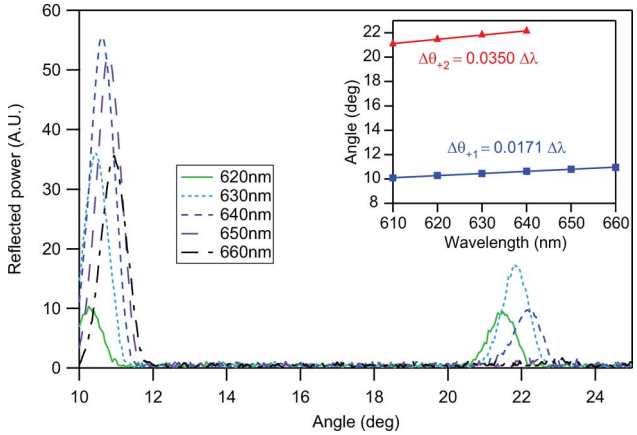


Fig. 3. (Color online) Plot of the reflectivity versus scatter angle for the binary reflection grating at an angle of incidence of 10° and various test wavelengths. In the inset, plot of the reflection angle as a function of the test wavelength for the first (blue squares) and second (red triangles) diffraction order. The lines are linear fits to the data.

microscope overview of the 150 $\mu$m diameter deflecting mirror and Fig. 2(c) shows a scanning electron microscope image of the nonperiodic grating with period varying from 200 to 500 nm at 50% duty cycle.

As shown in Fig. 3, we used a broadband ellipsometer (J. A. Wollam Vase Spectrographic Ellipsometer) with a tunable light source to measure the scattering properties of the device at various incident wavelengths. The ellipsometer shines a tunable light source on the device and measures the scattered light at various angles. The minimum angular separation between the source and the detector of the ellipsometer is $\simeq$30°, so we chose the angle of incidence to be 10° in order to allow us to measure the first scattered order at $\simeq$10°. The main part of Fig. 3 shows a plot of light intensity versus the scattering angle (measured relative to specular reflection). The light is strongly scattered in the first order with a weaker scattering peak at the second order angle of 20°. Observe that at the design wavelength of 650 nm the second order scattering is effectively suppressed while the first order has maximum intensity. The inset of Fig. 3 shows the change in the reflection angle as a function of the incident wavelength. The grating dispersion is equivalent to that of a grating of period 3.4 $\mu$m, and is in agreement with the period of the superstructure shown in Fig. 2(c). The ellipsometer does not allow us to measure the power in all diffraction orders (in particular the zeroth order of specular reflection) so we set up a measurement using a laser (New Focus Velocity, 640 nm) at an angle of incidence of $\simeq$5°. Table 1 shows the result of the measurement. Consistent with our model of the as-built grating, the largest amount of power is directed in the first order with some power left in the zeroth order due to the flattened phase profile of the grating. The other orders combined contain approximately 5% of the power.

We have introduced an application of GMR to blazed binary diffraction gratings. These gratings can be built using a straightforward lithographic process and, therefore, at scale, are much more economical to build than ruled gratings. The grating efficiencies reported here (44% in the first diffraction order) are not competitive with the best ruled grating on the market with efficiencies up to 80%. As mentioned before, the binary grating efficiency is hampered by limitations of our fabrication equipment. These limitations can be easily overcome using standard deep UV lithography. The 30 nm bandwidth experimentally observed in our grating does not compare favorably with the <100 nm bandwidth of commercial blazed gratings; further optimization of this parameter is a topic of current research. Given the flexibility of the fabrication technique it is also possible to build curved diffraction gratings with high NAs and polarization-insensitive gratings with a process that is identical to the one described here. In addition, we have shown that silicon GMRs can be used for visible wavelengths, provided that the gratings parameters are appropriately chosen. We believe that this new technology can have numerous scientific and commercial applications.

## References

1. R. Magnusson and S. S. Wang, Appl. Phys. Lett. **61**, 1022 (1992).
2. C. Mateus, M. Huang, Y. Deng, A. Neureuther, and C. Chang-Hasnain, IEEE Photon. Technol. Lett. **16**, 518 (2004).
3. S. M. Rytov, Zh. Eksp. Theor. Fiz. **29**, 605 (1955).
4. M. Huang, Y. Zhou, and C. Chang-Hasnain, Nat. Photon. **1**, 119 (2007).
5. D. Fattal, J. Li, Z. Peng, M. Fiorentino, and R. G. Beausoleil, Nat. Photon. **4**, 466 (2010).
6. F. Lu, F. Sedgwick, V. Karagodsky, C. Chase, and C. Chang-Hasnain, Opt. Express **18**, 12606 (2010).
7. P. Lalanne, S. Astilean, P. Chavel, E. Cambril, and H. Launois, J. Opt. Soc. Am. A **16**, 1143 (1999).
8. S. S. Wang, R. Magnusson, J. S. Bagby, and M. G. Moharam, J. Opt. Soc. Am. A **7**, 1470 (1990).
9. L. Li, J. Opt. Soc. Am. A **14**, 2758 (1997).